Chapter 17

Single-Molecule Imaging Measurements of Protein-Protein Interactions in Living Cells

Kayo Hibino, Michio Hiroshima, Yuki Nakamura and Yasushi Sako

Additional information is available at the end of the chapter

http://dx.doi.org/10.5772/52386

1. Introduction

Even though we have several techniques, represented by the electron microscopy, to obtain images of single molecules, in this chapter, we use 'single-molecule imaging' (SMI) for a limited means—that is, imaging of fluorescently labeled biological molecules at work for analyzing their behaviors. To observe biological molecules at work, imaging in aqueous conditions is essential. Therefore, optical microscopy is the main technology in SMI. Fluorescence labeling is good to use for imaging in optical microscopy, because it allows high contrast and selective imaging of molecules that we are interested in. SMI provides information of dynamics and kinetics of molecular reactions. In 1995, two groups firstly and independently realized SMI of biological molecules in aqueous conditions [1,2]. In the early days, SMI was used mainly for the *in vitro* studies of protein motors [1,2] and metabolic enzymes [3]. Detection of enzymatic reaction (reaction kinetics) [1,3] and detection of protein dynamics (lateral and rotational movements) [2] have been the two main usages of SMI since the first development of this technology. After that, the application of SMI has been extended, and in 2000, SMI became to be used in living cells [4,5].

Probably, for the readers, the most familiar usage of SMI is the measurement of molecular dynamics, including conformational changes and lateral and rotational movements. However, kinetic analysis is one of the original applications of SMI as mentioned above, and in many cases, it relates more closely to the higher-order biological functions than does dynamics analysis. This chapter focuses on the kinetic analysis of protein-protein interactions, including molecular recognitions and enzymatic reactions in living cells. As the application of SMI, we introduce a ligand-receptor interaction on the cell surface, and a process of protein activation occurs in a ternary protein complex beneath the plasma membrane. Because

the main subject of this chapter is the technical issue, these two examples of applications are chosen to explain how to analyze single-molecule data to understand kinetics of molecular interactions quantitatively in living cells. At the present time, we have several textbooks specialized for the technologies and applications of SMI in a wide field [6-8]. Please refer to these books for information lacking in this chapter.

2. Motivation of Single-molecule Imaging Measurements of Molecular Interactions

2.1. Single-molecule versus ensemble-molecule measurements

Before considering about technological issues, it might be important to discuss why we need SMI measurements of molecular interactions. The operation of biological molecular machines is basically stochastic. Therefore, in ensemble average measurements, in which only the averages over a huge number of reaction events are observed, details of the reaction process are obscured. In SMI measurements, it is possible to virtually synchronize a particular point in the reaction process for kinetic analysis. For example, imagine the observation of an enzyme reaction. The substrate solution is added to the enzyme solution to start the reaction. In ensemble measurements, the time of the two solutions mixing is set to time 0, and the concentration of the product is monitored with time. In the mixture, first, a substrate molecule needs to diffuse and collide with an enzyme molecule to form an enzyme-substrate (ES) complex; then, a chemical reaction starts on the enzyme molecule. The time 0 in ensemble measurements is not the time of ES complex formation. The time of ES complex formation is different for each molecule due to the stochasticity of molecular reactions, and this difference obscures the measurements of chemical reactions. In SMI measurements, the time point of each ES complex formation is detected, and after the observation, all the time points for individual molecules are aligned to time 0. Hence, in SMI measurements, we selectively extract the process of chemical reactions, removing the diffusion and collision for kinetic analysis.

This principle of SMI measurements also allows separation of forward and backward reactions. Here, imagine an association-dissociation reaction between two species of molecules. In the reaction mixture, both association and dissociation occur in parallel (on the different molecules). Even if we monitor the initial process of complex formation soon after the mixing of the two solutions, it is impossible to separate forward and backward reactions completely, and in the equilibrium, it is absolutely impossible to measure reaction kinetics, at least when the numbers of molecules are large. In SMI measurements, each association or dissociation event is detected individually; therefore, after the observations, association (or dissociation) events can be selected for pure kinetic analysis of association (dissociation) reactions. Because of this, kinetic analysis based on SMI, is possible, even in the equilibrium (or steady state) conditions.

Structures of biological macromolecules, especially proteins, often show multiple metastable points (this phenomenon is called polymorphism). Each single molecule is drifting among

http://dx.doi.org/10.5772/52386

these metastable points in various timescales. post-translational modifications, such as phosphorylation, may stabilize one or some of the metastable structures, according to each single molecule. SMI measurements are good to detect distributions and fluctuations of reactions and structures caused by static and dynamic polymorphisms of biological macromolecules [3,9-11]. In some cases, non-random reactions of proteins have been detected using SMI [3,9,11].

2.2. Single molecule measurements in living cells

In a cellular context, it is difficult to perform long time-series analyses of the reaction on the same single molecules due to high density and lateral movements of the molecules. However, SMI measurements still have advantages over conventional ensemble average measurements. SMI allows *in situ*, non-destructive quantitative measurements. SMI measurements provide absolute values of the kinetic and dynamic parameters of the molecular reactions and dynamics, including number, density, reaction rate constants, lateral diffusion coefficient, and transport velocity, with the smallest disruption of the living cell systems [8,12,13].

As mentioned above, for the time-series analyses, SMI measurements do not require physical synchronization, which is indispensable in ensemble molecule measurements. Synchronization, like concentration or temperature jumps, generally alters the condition of cell cultures, possibly affecting many cellular reactions in addition to the subject of the experiment. Therefore, it sometimes becomes ambiguous if the changes of the measured value reflect the reaction kinetics itself or the cellular dynamics triggered by the changed culture conditions. SMI measurements allow kinetic analysis in steady state, avoiding changes of culture conditions. For example, Hibino et al. [14] measured dissociation kinetics between two protein species, Ras and RAF, using SMI in quiescent cells in a steady state.

SMI measurements can detect small numbers of reactions in a limited volume inside living cells, because they are based on imaging with spatial resolution and possess the extreme sensitivity to detect single molecules. Using SMI measurement, Ueda et al. [15] measured the numbers and rate constants of the reactions between cAMP and its receptor, comparing the front and rear halves of a single *Dictyostelium* amoeba during chemotaxis. Tani et al. [16] analyzed reaction kinetics at the growth cone of nerve cells. These works have revealed that kinetic parameters of the same reactions diverged according to the positions in single cells. In addition, SMI measurements have directly revealed that cellular responses, such as neurite elongation [16] and calcium response [17], are caused by signaling of tens or hundreds of protein molecules.

The range of application of SMI measurements is broad, covering various fields of biological sciences of cells, including not only basic biochemistry and biophysics but systems biology, pathology of genetic diseases, action points analyses in pharmacology, and toxinology. SMI measurements provide absolute values of reaction parameters, which can be substituted into the reaction models described using mathematical equations. Since these values are determined in live cell conditions, SMI measurements are good to use in combination with mathematical modeling constructed to explain and predict dynamics of complex intracellular reaction networks.

3. Technologies of Single-molecule Imaging in Living Cells

3.1. Microscope and imaging equipment

SMI uses optical microscopy, and since most of the biological molecules are translucent for visible light, some kind of labeling is required. For detection of single molecules, labeling with fluorophore is effective, because it provides high-contrast imaging, which is essential both for detection of small signals from a single molecule and for detection of specific species of molecules in crowded conditions of living cells. Labeling by fluorescent proteins has expanded the application of SMI in living cells.

Fluorescence signal from single fluorophores is small but enough to be imaged individually when recent high-sensitivity video cameras, like EM-CCD or CCD equipped with a multichannel plate image intensifier are used. Standard temporal resolution of SMI in living cells is several tens of ms, and in some cases, under strong illumination, ms sampling has been achieved gathering hundreds of photons from a single fluorophore per single video frame.

For detection of small signals from single molecules, background rejection is essential. Total internal reflection [1] and oblique illumination [18] are useful technologies of wide-field fluorescence microscopy to realize effective background rejection and can be used for SMI in living cells (Figure 1) [19].

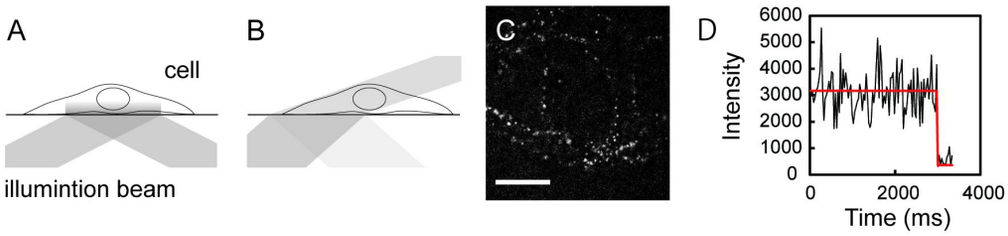

Figure 1. Single-molecule imaging in living cells. Schemes of total internal reflection (A) and oblique illumination (B) microscope and a single-molecule image of tetramethylrhodamine-labeled EGF on the surface of living HeLa cells under an oblique illumination microscope (C) are shown. Bar in C: 10 μm. Detection of singlemolecules can be examined by single-step photobleaching (D).

Figure 2 shows the optical setup of our TIR microscope for SMI, which was home-built based on a commercial inverted fluorescence microscope. Solid-state continuous wave lasers in different emission wavelengths are used for illumination according to the species of fluorophore. Between the lasers and the microscope, a two-dimensional beam scanning system is constructed. This system is composed by a pair of diagonallypositioned Galvanometer-scanning mirrors and a telescope that inserted between the two scanning mirrors. The two scanning mirrors are moved sinusoidally with a π phase difference in a frequency higher than the frame rate of imaging (30 Hz is the typical frame rate). Therefore, the specimen is illuminated from every direction during the acquisition of single frames. Thus, the system achieves pseudo-circular illumination.

Circular illumination is better in TIR-microscopy than the illumination from a fixed single direction that is usually used in commercial TIR system, especially for observations of biological samples having anisotropic structure [19]. It also reduces effects of spatially inhomogeneous illumination pattern often caused by the strong coherence of laser beams. There are several methods to construct circular illumination path using only static optical elements or a rotatory moving mirror with a fixed angle, however, using a pair of Galvanometer, the incident angle of the illumination beam to the specimen is easily adjusted to the best position for each specimen by changing the amplitude of vibration of the scanner mirrors.

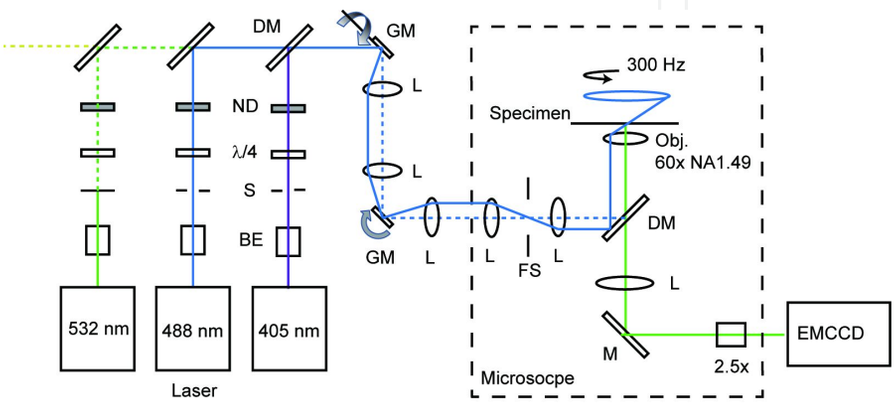

Figure 2. Optical path of a total internal reflection fluorescence microscope for single-molecule imaging.The illumination laser beams are introduced into an inverted fluorescence microscope from the epi-illumination path. Between the microscope and lasers, a two-demensional beam scanning system is inserted to achieve pseudo-circular illumination (see text for details). The violet (405-nm) laser is used for photoconversion of fluorophores. BE: beam expander, DM: dichroic mirror, FS: field stop, GM: Galvanometer scanner mirror, L: lens, λ/4: quarter wave plate, M: mirror, ND: neutral density filter, S: shutter.

3.2. Fluorophores

Both the chemical fluorophores and fluorescent proteins are applicable as the probes of SMI in living cells. To obtain good contrast against autofluorescence of cells and optics, fluorophores with relatively longer wavelength emissions are generally better. As the chemical fluorophores, tetrametylrhodamine (TMR), Cy3, Cy5, Alexa 488, and Alexa 594 are used frequently. Among the fluorescent proteins, as far as we know, eGFP is the best for SMI because of relatively good photostability. As the red fluorescent protein in SMI, tag RFP is applicable. Photoconvertible proteins, Eos and mKikGR, are good in photoactivation localization microscopy (PALM), which is an application of SMI [20]. Protein tags, like HaLo and SNAP, which can be conjugated covalently with chemical fluorophores after expression in living cells, are useful, because chemical fluorophores are generally more photostable than the fluorescent proteins, and colors of fluorescence emission can be changed according to the purpose of the experiment. When an especially strong and stable (long observation time) signal is required, Q-dot or other fluorescent beads will be used. In such cases, steric hindrance and multivalency should be controlled carefully.

3.3. Sample preparation

For SMI, cells are cultured on a coverslip and set on the microscope. Since contamination of small dust on the coverslip prevents SMI, the coverslip must be washed thoroughly before transfer of cells onto it [21]. Usage of glass coverslips (not conventional plastic cell culture dishes) that has the high refractive index was necessary to achieve total internal reflection; however, some cell culture dishes or chambers made of plastic with the refractive index similar to that of glass (1.52) can be purchased recently. One day or more before the observation, the culture medium should be replaced to one that does not contain phenol red to reduce background fluorescence. The culture medium used during observation should also not contain phenol red.

When proteins tagged with fluorescent proteins, like GFP, are expressed and observed in cells, conditions for the transfection of cDNAs should be carefully controlled to avoid overexpression that prevents SMI (see section 3.5). Similarly, when HaLo or SNAP tag is used, staining should be carried out with a much lower concentration of fluorescent regents than that recommended by the manufactures.

3.4. Image processing

The signal-to-noise ratio (S/N) in SMI is usually not good due to small signals and, especially in cells, due to rather large background autofluorescence and scattering. Temporal averaging over successive video frames improves S/N under the sacrifice of temporal resolution. Spatial filtering of the images is also used to improve image quality. But, one must be careful to use any temporal and spatial filtering, because they sometimes do not preserve the linearity of signal intensity. Background subtraction is usually carried out before quantification of single-molecule signals. In cells, because background signals are highly inhomogeneous, the background levels should be determined locally.

After the appropriate pretreatments, the position and signal intensity are determined for individual single-molecule images. For this purpose, fitting with a two-dimensional Gaussian distribution is usually used. Fitting functions can include background signals instead of the pretreatment of background subtraction. We usually use a Gaussian distribution on an inclined background plane as the fitting function [21]. Positions of the molecule can be determined as the centroid of the distribution with sub-pixel spatial resolution. Signal intensity can be calculated by integration of the distribution function. Accuracy of these parameters depends on the measurement system and should be determined statistically from the repeated measurements of the same single molecules.

There are several criteria to judge whether single molecules are really detected or not [4]. Single-step photobleach is the most convenient and used criterion (Figure 1D). To distinguish photobleach from disappearance by the movements of molecules, like release into the solution, illumination intensity should be changed. Photobleaching rate, but not the rate of most of other phenomena, depends on the illumination intensity. Because the size of fluorophores is much smaller than the spatial resolution of the optical microscope, the profile of single-molecule images must be the point spread function of the optics. The intensity distri-

bution of single molecules should be Gaussian, because the photon emission from a fluorophore is a Poisson process; however, when the intensities are small, the distribution becomes binominal or sometimes looks as a log-normal distribution.

3.5. Technical limitations specific for SMI

Photobleach of the fluorophore seems to be the most serious problem in SMI. This brings a trade-off between S/N of the single-molecule measurments and the observation length of each single molecule. By increasing the illumination power, the signals from single molecules increase to improve S/N, which in turn improves the temporal resolution and the accuracy of position determination; however, at the same time, the observation length of each single molecule must be decreased due to increased photobleacing rates. In typical conditions, the emission photon numbers from a single chemical fluorophore, including TMR and Cy3, before photobleach is less than 1 million, and those from fluorescent proteins are several times smaller. Since SMI in typical conditions requires thousands of photon emissions from a fluorophore per frame (due to limited numerical aperture of the objective and tranmittance of the optics, <10% of which reach to the camera), only hundreds of frames can be acquired for each single molecule. If a video rate movie is taken, single molecules could be observed only for about 10 s in average.

Signal intensity (photon flux) of single fluorophores is limited, because the fluorescence emission cycle requires a finite time. The fluorescence lifetime, which is the rate-limiting parameter under strong enough illumination, of typical fluorophores used in SMI is about 1 ns, meaning that the maximum photon flux is about 10^9 s^{-1}. However, strong illuminations that cause such high-rate emission induce higher-order excitation that could be the reason of undesired photochemical reactions. Practical photon emission rate is no more than about 10^6 s^{-1}. This means that because thousands of photons are required to acquire a snapshot of SMI, temporal resolution of SMI is difficult to be improved to more than 1 ms. Accuracy of position detemination depends on the signal intensity. When more than 10,000 photons are obtained on the camera for a single frame, the centroid of a single-molecule image can be determined with 1 nm of accuracy [22]. Such high accuracy cannot be obtained with a temporal resolution better than subseconds.

The special resolution of the optical microscopy is worse than 200 nm. This limits the densities or the concentrations of the molecule to be observed, because in dense conditions, images of molecules overlap to inhibit single-molecule detection. The practical limits of the molecular density and concentration are about 10 μm^{-2} and 10 nM, respectively. Concentrations of most cell signaling proteins are thought to be within these limits, but those of structural proteins could exceed these limits.

4. Applications and DetaAnalysis

4.1. Single-molecule kinetic analysis

4.1.1. Principle

Durations and intervals of molecular interactions contain information about reaction kinetics. Hereafter, we call the durations of the colocalization of two molecules as 'on-times', and the intervals from the dissociation of two molecules to the association of the next molecule with one of the dissociated two molecules as 'off-times'. On-times and off-times can be measured for single events using SMI. Dual-color SMI (Figure 3) is possible to detect on-times, but in practice, due to photobleach, it is difficult to detect successive multiple on-times for a single molecule and not easy to detect even a single off-time.

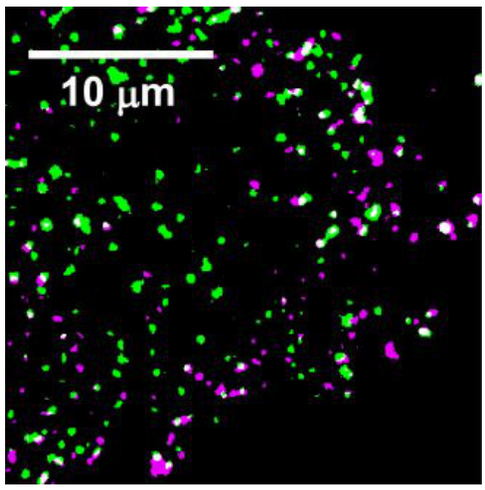

Figure 3. Dual-color single-molecule imaging of TMR-labeled epidermal growth factor (EGF; magenta) and GFP-Sos (green) in a living HeLa cell. Basal cell surface was observed using a dual-colour total internal reflection fluorescence microscope. EGF receptors (EGFR) on the cell surface are activated by EGF binding. Then, Sos molecule,complexed with Grb2, associates to the activated EGFR. White spots represent the EGF-EGFR-Grb2-Sos complexes in the plasma membrane.

More practical single-molecule measurements of on- and off-times are achieved for the interactions between a soluble molecule and a molecule stably attached on stationary structures. Because of the rapid Brownian movements in solution, soluble molecules cannot be observed as clear fluorescent spots and can only be imaged when they associate with fixed or slowly moving molecules. Therefore, *in vitro* SMI measurements, interactions between fluorescently labelled soluble molecules and a (non-labeled) molecule fixed on the substrate are often observed [1, 11]. In such cases, because different soluble molecules interact with a fixed molecule in turn, photobleach has minimal effect. Similar measurements can be achieved in living cells when interactions are observed between a fluorescently labelled soluble molecule (either in the extracellular solution or in the cytoplasm) and molecules in the membrane or cytoskeleton structures. Inside living cells, detection of the successive on-times as well as the single off-time is difficult by this way because of the movements and/or high

density of the non-labeled molecules. However, even in living cells, measurements of the waiting times of the first association after some perturbation and measurements of off-times are usually possible for kinetic analyses.

4.1.2. Estimation of the reaction parameters

Consider a reaction of state change,

$$A \xrightarrow{k} \phi \tag{1}$$

Here, A and ϕ represent association and dissociation states, respectively, for example, and then k is the dissociation rate constant. The on-time distribution, which is the normalized histogram to show the fraction of on-times observed in each time interval from t to $t+\Delta t$, means changes of the nomarlized frequency to observe disappearance of the association state as a function of time. In other words, the on-time distribution represents the reaction rate to produce the dissociation state with time after the formation of the association state. (Disappearance of A state is the appearance of ϕ state in the reaction equation (1).)

Hence, the on-time distribution is the reaction rate equation,

$$\frac{d\phi(t)}{dt} = kA(t). \tag{2}$$

Here, the reaction is assumed to proceed according to a simple mass action model. Different from the kinetic analyses in conventional biochemical techniques that deal with the concentration changes, the reaction rate equations in SMI describe state changes of a single molecule with time; i.e., in equation (2), $A(t)$ and $\phi(t)$ do not mean the concentrations but the probabilities with which each of the states is observed. Because every single molecule takes one of the two states in this reaction model, and because at the starting point of each on-time the molecule takes A state, equation (2) has a conservation condition; $A(t) + \phi(t) = 1$, and the initial condition; $A(0) = 1$. Under these conditions, equation (2) is solved as $A(t) = \exp(-kt)$. Then,

$$\frac{d\phi(t)}{dt} = kA(t) = k \exp(-kt). \tag{3}$$

By fitting the on-time distribution with equation (3), the best-fit value for k is obtained.

This procedure is similar to that used in a conventional biochemical analysis based on ensemble-molecule measurements. However, there are two major different points between SMI and ensemble-molecule analyses. First, the initial condition $A(0) = 1$ is not always applicable in ensemble-molecule analysis. Second, and more importantly, in SMI analysis, the forward and backward reactions can be analyzed completely separately. In the presence of many molecules in the reactant, the association and dissociation reactions take place in parallel; therefore, in ensemble molecules, the reaction equation should be

$$\mathrm{A} \underset{k_{-}L}{\overset{k_{+}}{\rightleftarrows}} \phi. \tag{4}$$

Then, the rate equation is

$$\frac{\mathrm{d}\phi(t)}{\mathrm{dt}} = \mathrm{k}_{+}A(t) - k_{-}L\ \phi(t). \tag{5}$$

Here, L means the concentration of the ligand molecule, which can be thought of as a constant in the presence of excess amount of the ligand. The solution for $A(t)$ under the same conditions, $A(t) + \phi(\mathrm{t}) = 1$ and $A(0) = 1$, is

$$A(t) = \frac{k_{+}}{k_{+} + k_{-}L} \exp\{-(k_{+} + k_{-}L\ )t\} + \frac{k_{-}L}{k_{+} + k_{-}L}, \tag{6}$$

indicating that the association (k_{+}) and dissociation (k_{-}) rate constants are never able to determined independently by fitting to a timecourse describing the concentration change of A state. (In ensemble-molecule measurements, obtaining multiple timecourses by changing the ligand concentration, L, the association and dissociation rate constants can be determined separately. However, in this case, there is an additional assumption that the rate constants are independent of the concentration.)

Reactions are not always as simple as described in equation (1). Multi-component reactions, described by a sum of exponential functions, are usual for proteins [11,15]. Also, reaction intermediates are sometimes involved. Such reaction structures could be noticed from the shape of the on(off)-time distributions. For example, sequential dissociations of two binding sites in a single molecule are described by the tandem reaction model [14],

$$\mathrm{A} \overset{k_1}{\rightarrow} \mathrm{B} \overset{k_2}{\rightarrow} \phi \tag{7}$$

Here, ϕ state is the off state again,and the on-time distribution is

$$\frac{\mathrm{d}\phi(t)}{\mathrm{dt}} = k_2 B(t). \tag{8}$$

At the same time,

$$\frac{\mathrm{d}A(t)}{\mathrm{dt}} = -k_1 A(t), \tag{9}$$

and

$$\frac{dB(t)}{dt} = k_1 A(t) - k_2 B(t). \quad (10)$$

Solving the coupled differential equations (8-10) under the conditions $A(t) + B(t) + \phi(t) = 1$, $A(0) = 1$, and $B(0) = \phi(0) = 0$,

$$\frac{d\phi(t)}{dt} = k_2 B(t) = -\frac{k_1 k_2}{k_1 - k_2}\{\exp(-k_1 t) - \exp(-k_2 t)\}. \quad (11)$$

This distribution is peaked; conversely, from the peaked distribution of on-times, presence of a reaction intermediate (or multiple intermediates) can be noticed. By fitting the on-time distribution by equation (11), two reaction rate constants can be determined. However, in this case, even two values of the rate constants are obtained, it is impossible to assign which one is the value of each rate constant, because k_1 and k_2 are interchangeable in equation (11). Additional experiments or information is required for the assignment.

4.1.3. spFRET measurements for detection of molecular interactions

In some case, more direct evidence for interactions between two species of single molecules should be required. Although the spatial resolution of optical microscopy is worse than 200 nm, the position (centroid) of each single-molecule image can be determined at nm-level resolution, if sufficient signal is obtained [22]. Dual-color SMI (Figure 3) allows detection of colocalization within several tens of nm in typical conditions. More accurate detection of direct molecular interactions is allowed by detecting single-pair FRET (spFRET) signal [4,23]. spFRET has a power to detect molecular interactions in crowding conditions, because FRET from sparsely distributed donors to dense acceptors yields sparse signal from the acceptors, which can be detected in single molecules [24]. However, usage of spFRET is limited due to its weakness to photobleach and difficulty to tuning labeling conditions to obtain high FRET efficiency.

4.2. Interactions between epidermal growth factor (EGF) and EGF receptor, and receptor dimerization

4.2.1. EGF and its receptor

Ligand-receptor interactions are one of the basic reactions in cell signaling systems. Here, we used SMI for detection of interactions between an extracellular ligand and receptor on the cell surface.

Epidermal growth factor, EGF, is a soluble cell signaling protein in the extracellular medium. EGF associates with its receptor, EGF receptor (EGFR), in the plasma membrane to stimulate cell proliferation [25]. EGFR is a single membrane spanning protein expressed in various types of animal cells. At the extracellular domain, an EGFR molecule associates with a single molecule of EGF; then, the conformational change of EGFR is thought to induce dimerization of two EGF-associated EGFR molecules. In addition to monomers of vacant

EGFR molecules, predimers of EGFR molecules (dimers without association of EGF molecules) are known to present on the cell surface. However, it is widely believed that only after formation of doubly liganded dimers (signaling dimers), EGFR molecules are activated through phosphorylation at the cytoplasmic domain. These phosphorylations are carried out through the mutual phosphorylations in the signaling dimers using the kinase activity in the cytoplasmic side of EGFR molecules (Figure 4). We tried to determine the kinetic process of EGF-EGFR associations and formation of signaling dimers of EGFR using SMI measurements [26,27].

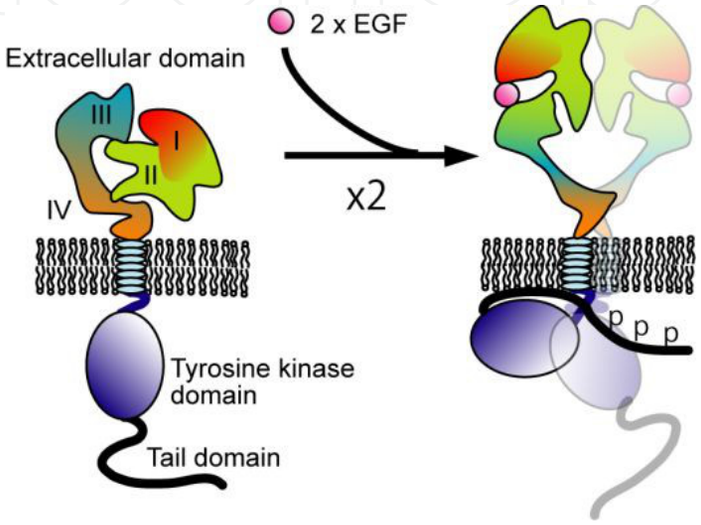

Figure 4. A schematic model of associations between EGF and EGFR and formation of signaling dimers of EGFR.

4.2.2. Single-molecule imaging of EGF association

EGF can be conjugated with chemical fluorophores like TMR at the N-terminus without disruption of its biological activity. After applications of nM orders of TMR-labeled EGF to the culture medium of cells under an oblique illumination fluorescence microscope, associations of single EGF molecules on the apical surface of living cells were observed in real time (Figure 1C). Movies of EGF associations were acquired in 20 frames/s. In this experiment, a human breast cancer cell line, MCF-7, was used. From the single-molecule movies, associations of single EGF molecules were detected individually as the sudden appearance of fluorescent spots on the cell surface (Figure 5A). When the association sites contained more than one EGFR molecule, the second associations were observed at the same positions of the first association sites. Some of the double association sites could be predimers of EGFR, and others could be two EGFR molecules presented in close proximity by accident. In our experimental conditions, no association site showed more than double association.

The association kinetics between EGF and EGFR were analyzed from the distributions of the waiting times for associations of single EGF molecules (Figure 5B,C). The waiting time distribution for the EGF association for the first EGF molecules could be described by a 2-component exponential function with rate constants of k_1 = 1.4 x 10^{-3}nM^{-1}s^{-1} and k_2 = 3.8 x 10^{-2}

http://dx.doi.org/10.5772/52386

$nM^{-1}s^{-1}$. The difference between two types of EGF association sites in the association rate constant of EGF has not been fully known, but it is possible that the latter (k_2) is the association rate constant of the first EGF molecule to the predimers of EGFR, because the association rate constant for the single association sites was the same as k_1 (Figure 5B).

The waiting time distributions for the second associations to the double association sites were peaked (Figure 5C). The distributions were analyzed using the tandem reaction model (equation 7). By changing the concentration of EGF, the rate constants for the intermediate formation (k_3) and for the association of the second EGF molecule (k_4) were assigned: k_3 was independent of the EGF concentration, suggesting that it was the rate constant for a conformational change induced by the first EGF association, while k_4 was proportional to EGF concentration, suggesting they were the association rate constants for the second association of soluble EGF molecules with the singly-liganded EGFR dimers. The values were k_3 = 4.0 s^{-1} and k_4/L = 2.4 $nM^{-1}s^{-1}$. The intermediate between the first and the second associations of EGF molecules was first detected using SMI. These results suggest that the association rate constant with EGF is increased by the formation of predimer of EGFR and, after the association of the first EGF molecule to the EGFR dimer, increased further. These properties of EGF-EGFR interactions facilitate the formation of signaling dimers of EGFR. Similar results were observed on HeLa cells [26] and other EGFR family members on MCF-7 cells [27].

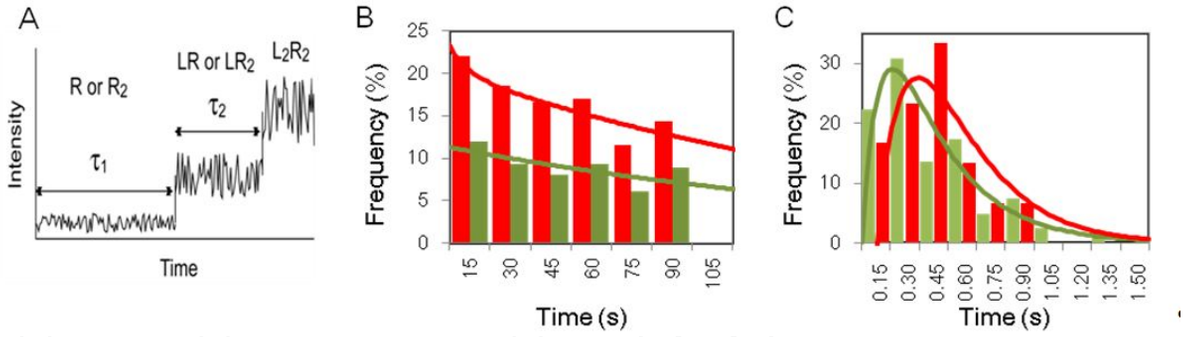

Figure 5. Single-molecule measurement of the associations between EGF and EGFR. (A) Single-molecule detections of the associations of EGF with EGFR are illustrated schematically. Waiting times of the association (appearance) of fluorescent spots on the cell surface (τ_1) were measured individually after the application of TMR-EGF to the cell culture medium. Second associations of TMR-EGF, which could be detected by a step-like increase of the fluorescence intensity, were observed in some association sites. The waiting times of the second association after the first association (τ_2) were also measured. (B) The distributions of τ_1 were measured for all association sites (red bars) and for the single association sites (green bars) in the presence of 4 nM TMR-EGF. The numbers of events were 57 (red) and 31 (green). Lines show the results of fitting with the reaction models. The red histogram was fitted with a two-component exponential function, suggesting the presence of two different association sites. The green histogram was fitted with a single-component exponential function. See text for the values of rate constants. (C) The distributions of τ_2 were measured in the presence of 2 nM (red bars) or 4 nM (green bars) of TMR-EGF. The numbers of events were 30 (red) and 81 (green). The distributions were analyzed by the tandem reaction model. In this model, the first and second steps are the state change and association of the second EGF molecule, respectively. Therefore, the reaction rate of the first step is independent to the EGF concentration, but the second step should be proportional to the EGF concentration. The best-fit values of the first-order reaction rate constants for the second step were 4.7 and 4.7 s^{-1} (2 nM), and 3.4 and 10 s^{-1} (4 nM), suggesting that the rate constant of the first step were 4.7 (2 nM) and 3.4 (4 nM) s^{-1}, and the

second-order rate constants were 4.7/2 (2 nM) and 10/4 (4 nM) $nM^{-1}s^{-1}$. The averages of the rate constants weighted with the event number are 4.0 s^{-1} and 2.4 $nM^{-1}s^{-1}$.

4.3. Interaction between a small GTPaseRaf and a cytoplasmic kinase RAF

4.3.1. Ras and RAF

As the second example of SMI kinetic analysis, intracellular molecular reactions of RAF were analyzed [14,28,29]. As a downstream signaling of EGFR, EGF stimulation induces activation of a small GTPase, Ras, on the cytoplasmic side of the plasma membrane. The active form of Ras is recognized by a cytoplasmic serine/threonine kinase, RAF, which is the MAPKKK of the RAF-MEK-ERK MAPK cascade; thus, RAF translocates from the cytoplasm to the plasma membrane upon activation of Ras (Figure 6A). The active form of Ras induces translocation of RAF but does not activate RAF directory. RAF activation was induced though phosphorylations by still undetermined kinase(s) on the plasma membrane. RAF contains two association sites for Ras (the Ras-binding domain RBD and the cysteine-rich domain CRD). In addition, RAF has at least two conformations, open and closed. In the closed form, due to intramolecular interactions, CRD and the catalytic domain (CAD) of RAF are covered from Ras and the kinase(s), respectively (Figure 6B). Thus, the kinetics of RAF activation in the ternary complex among Ras, RAF, and the kinase(s) should be complicated. Actually, the kinetics of RAF activation has not been known at all. It cannot be studied *in vitro*, since the kinase(s) is(are) not determined. However, in living cells, SMI measurement is applicable.

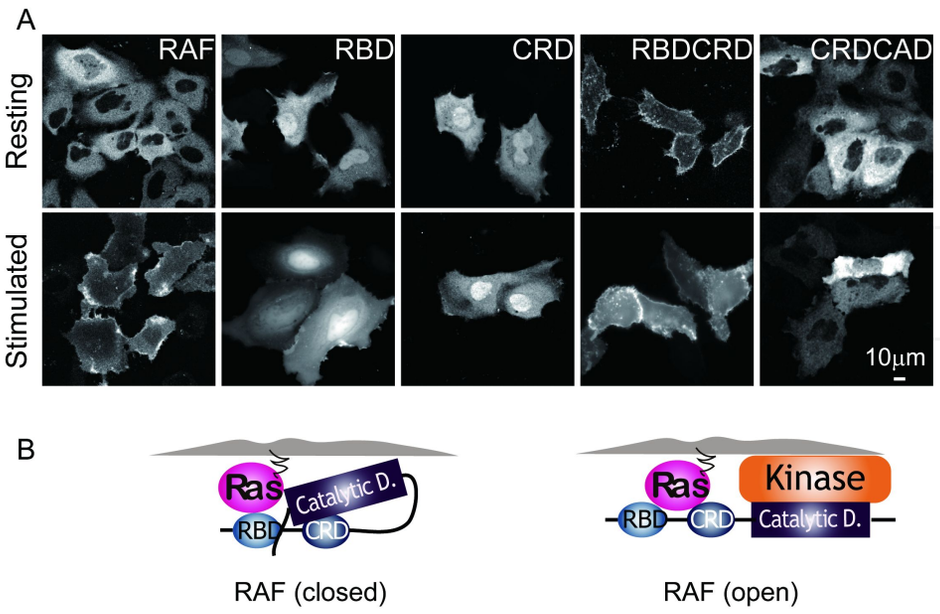

Figure 6. Translocation of RAF.(A) C-RAF1 and its fragments tagged with GFP at the N-terminus was expressed in HeLa cells and observed in ensemble-molecules before (upper panel) and after (lower panel) stimulation of cells with EGF. RAF (whole molecule) translocated from the cytoplasm to the plasma membrane. Translocation was not evident

for RBD, CRD, and CRD-CAD fragments. RBD-CRD fragments accumulated on the membrane independent of EGF stimulation. (B) RAF contains two Ras-association domains (RBD and CRD) and has two conformations (open and closed).

4.3.2. Single-molecule imaging of RAF translocation

C-RAF, which is a ubiquitous isoform of RAF, was tagged with GFP (GFP-RAF) and expressed in HeLa cells. GFP-RAF presented in the cytoplasm of quiescent cells and translocated to the plasma membrane upon activation of cells with EGF. The translocation of whole molecules of RAF was observed in ensemble-molecule imaging. Only a small amount of the RBD fragment of RAF showed translocation, and the RBD-CRD fragment bound to the plasma membrane independently of cell stimulation (Figure 6A). The RBD-CRD fragment with a mutation to inactive RBD (CRD) and a mutant of RAF in the open form with inactive RBD (CRD-CAD) did not show remarkable translocation to the plasma membrane in ensemble molecules, even after EGF stimulation.

Reducing the expression levels of GFP-tagged molecules, single molecules of RAF and its fragments were observed on the plasma membrane (Figure 7). For all molecules, transient associations with the plasma membrane were observed in single molecules after EGF stimulation, and for the molecules containing RBD (RAF, RBD, and RBD-CRD), associations of a small amount of molecules were observed, even in quiescent cells. The densities of membrane-associated molecules increased with overexpressions of Ras, suggesting Ras-specific membrane interactions of RAF molecules.

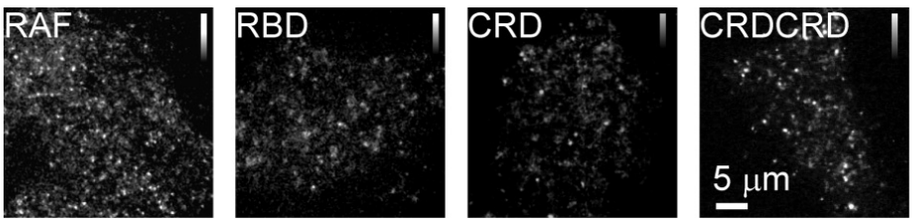

Figure 7. Single-molecule images of RAF and RAF fragments in HeLa cells. These images were observed in a HeLa cells 2-5 min periods after stimulation with EGF.

4.3.3. Kinetic analysis of RAF activation

On-time distributions of RAF molecules were obtained in cells after EGF stimulation (Figure 8A). RBD and CRD showed single exponential on-time distributions with the decay rate constants of 3.8 and 2.4 s^{-1}, respectively. Because the decay of on-time distributions is determined by both dissociation and photobleach as the reasons of disappearance of the fluorescent spots, the decay rate constants are the sum of the rate constants for dissociation and photobleach. After the corrections for the photobleaching rate constant, which was determined by SMI in fixed cells, the dissociation rate constants for RBD (k_1) and CRD (k_2) were determined as k_1 = 3.7 and k_2 =2.3 s^{-1}, respectively. Corrections of photobleach were also carried out in the following analyses (see supplement information of [28] for details). The on-time distribution of RBD-CRD was peaked, suggesting sequential dissociation of RBD and

CRD from Ras. Association with Ras using both RBD and CRD could induce firm membrane anchoring of RBD-CRD, even in the quiescent cells. Applying the dissociation rate constants of RBD and CRD, the on-time distributions of RBD-CRD could be described by the following reaction model [29]:

$$RC \underset{k_{1-}}{\overset{k_1}{\rightleftarrows}} C \xrightarrow{k_2} \phi. \tag{12}$$

In this scheme, RC or C represents the state in which the molecule associates with Ras using both RBD and CRD, or only CRD, respectively. Since it is known that CRD of Ras molecules associates with Ras very rapidly after the association of RBD to Ras [14], R state (in which the molecule associates with Ras only with RBD) was neglected in this reaction scheme. Using this scheme, k_{1-} (the association rate constant between RBD and Ras from the C state) was determined to be 1.0 s^{-1}.

RAF and CRD-CAD interact with the kinase(s) on the plasma membrane as the substrate. In addition, RAF contains open-close dynamics. Our previous study using spFRET [14] indicated that the initial association form of RAF with the activated Ras (in our time resolution of ~0.1 s) is an open conformation. The reaction model (equation 12) was extended to include the phosphorylation by the kinase.

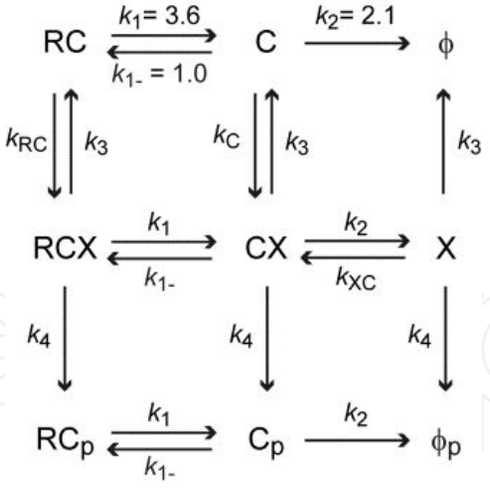

(13)

Here, for simplification, phosphorylation of RAF was assumed to be a single Michaelis-Menten type reaction. Suffixes X and p mean that each state forms complexes with the kinase(s) and is phospholylated, respectively. For the CRD-CAD fragment, RC, RCX, and RCp are not applicable.

Numerically solving the coupled differential equations for the time-dependent probability changes of the molecular states, functions to describe the on-time distributions of RAF and CRD-CAD were calculated and fitted simultaneously to the results of experiments to find the best-fit values of the rate constants. The results are shown in Figure 8B. The deformation of the RAF-kinese complex without enzymatic reaction was slow ($k_3 < 10^{-4}$ s^{-1}) and negligible, and the complex formation mostly took place from the RCX state, not from the C state. The large difference between the rates of complex formation with the kinase from the RC (47 s^{-1}) and C (0.6 s^{-1}) states suggests that interactions with Ras at the RBD and CRD coordinately work for effective presentation of RAF to the kinase. The very rapid association between RAF in the RC state and the kinase to form the RCX complex suggests a preexisting complex between Ras and the kinase. Simulation using the parameters determined by this analysis predicted that once associated with Ras, 95% of RAF molecules are released to the cytoplasm in the phosphorylated (active) form. Thus, efficiency of phosphorylation on the plasma membrane is high, and the overall activation level of RAF in cells should be regulated by the translocation from the cytoplasm to the membrane and/or dephosphorylation in the cytoplasm.

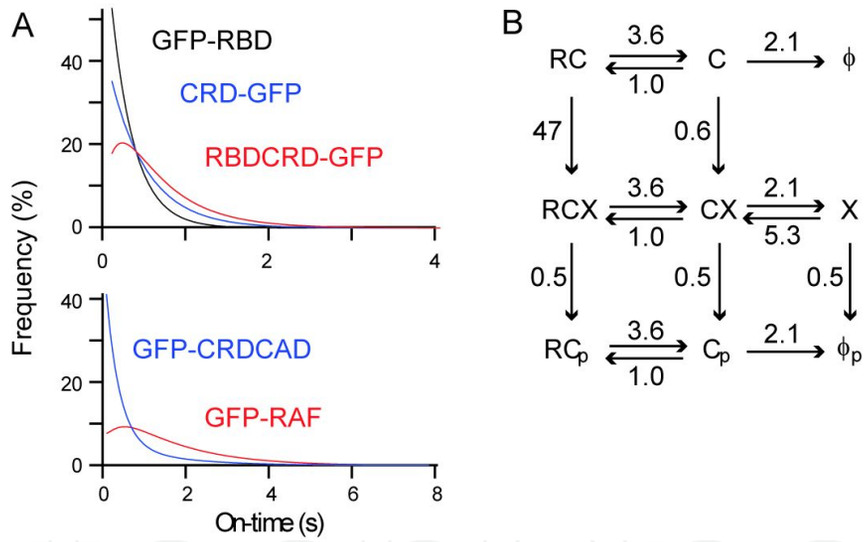

Figure 8. Single-molecule analysis of RAF activation. On-time distributions of RAF and fragments of RAF were analyzed. Results of fittings with the kinetic models are shown (A). The best-fit values of the reaction rate constants (s^{-1}) were determined (B).

4.4. Applications in toxinology

Kinetic analysis of the protein-protein interactions using SMI is a general technology, and there have already been several examples in toxinology. *Staphylococcus aureus* leukocidin fast fraction (LukF) and γ-hemolysin second component (HS) assemble into hetro-oligomeric pores of γ-hemolysin on the cell surface to induce cell lysis. Detecting spFRET between LukF and HS, Nugyen et al. [24] have succeeded in determining equilibrium dissociation constants between the molecules in the intermediate complexes during the pore formation.

A hydrophobic environmental sensitive fluorophore, badan, labeling LukF, has also been used to detect complex formation with HS in single molecules [30].

Groulx et al. [31] measured the stoichiometry of oligomerization of another pore-forming toxin using SMI. Monomers of *Bacillus thuringiensis* toxin Cry1Aa were labeled with a fluorophore at a cysteine residue. After the complex formation, molecules were attached on a coverslip to observe the photobleaching process. Counting the step number during the photobleach, it was concluded that the toxin forms a tetramer.

Nabika et al. [32] used SMI for observation of lateral diffusion of cholera toxin B subunit (CTX) on the artificial lipid bilayer containing GM1, which is the receptor of CTX. The diffusion coefficient was one order smaller than that of lipid molecules in the membrane, and there were higher (0.4 $\mu m^2/s$) and lower (< 0.1 $\mu m^2/s$) diffusive fractions. This observation was explained by assuming multivalent binding between CTX and GM1 molecules.

On the contrary, toxin has been used for single-molecule measurement. Since direct fixation of molecules to a substrate possibly induces artifacts in the measurements, single molecules are sometimes entrapped into fixed tiny liposomes in which the molecules can move more freely. In this case, however, the solution around the molecules cannot be changed during the experiment, limiting experimental conditions. Okumus et al. [33] used liposomes, reconstituting pore-forming toxin, to allow exchange of inside solutions.

5. Conclusions

As shown in this chapter, SMI can be used to detect molecular interactions between proteins and other biological molecules. In addition to detections of static oligomerization states, SMI allows characterization and analysis of dynamic reaction processes, including association-dissociation kinetics and enzymatic reactions.

Kinetic analyses based on SMI measurements have several advantages over analyses using conventional biochemical and ensemble-molecule imaging measurements: SMI allows quantitative measurements with minimal disruption of the system integrity. Actually, SMI is applicable to complex systems, like living cells, and avoids perturbations for synchronization. Measurements in complex systems are useful in analyses of the reaction kinetics between unknown elements, as shown in the case of RAF and the undetermined kinase(s). SMI measurements have often found novel reaction intermediates. This is because virtual synchronization at the reaction steps and complete separation between the forward and backward reactions are allowed.

These advantages of SMI measurements make them effective in quantitative analysis of biological reaction kinetics, providing basic information required in system-level analyses in recent molecular cell biology. In the near future, SMI measurements will be expanded to be used in pharmacology to provide novel drug screening methods and analyses of the sites of action for medical drugs, in pathology to detect currently undetermined dysfunctions of

pathological mutant molecules, and in toxinology for the analyses of molecular mechanisms of toxic functions.

Author details

Kayo Hibino[1], Michio Hiroshima[1,2], Yuki Nakamura[2] and Yasushi Sako[2*]

*Address all correspondence to: sako@riken.jp

1 Laboratory for Cell Signaling Dynamics, RIKEN QBiC, Japan

2 Cellular Informatics Laboratory, RIKEN. 2-1 Hirosawa, Japan

References

[1] Funatsu, T., Harada, Y., Tokunaga, M., Saito, K., & Yanagida, T. (1995). Imaging of single fluorescent molecules and individual ATP turnovers by single myosin molecules in aqueous solution. *Nature*, 374, 555-559.

[2] Sase, I., Miyata, H., Corrie, J. E. T., Craik, J. S., & Kinosita, K. Jr. (1995). Real time imaging of single fluorophores on moving actin with an epifluorescence microscope. *Biophys J*, 69, 323-328.

[3] Lu, H. P., Xun, L, & Xie, X. S. (1998). Single-molecule enzymatic dynamics. *Science*, 282, 1877-1882.

[4] Sako, Y., Minoguchi, S., & Yanagida, T. (2000). Single molecule imaging of EGFR signal transduction on the living cell surface. *Nat Cell Biol*, 2, 168-172.

[5] Shütz, G. J., Kada, G., Pastuchenko, V. Ph, & Schindler, H. (2000). Properties of lipid microdomains in a muscle cell membrane visualized by single molecule microscopy. *EMBO J*, 19, 829-901.

[6] Selvin, P. R., & Ha, T. (2008). Single-molecule techniques. *A laboratory manual. Cold Spring Harbor Laboratory Press New York*.

[7] Yanagida, T., & Ishii, Y. (2009). Single molecule dynamics in life science. *WILEY-VCHWeinhim*.

[8] Sako, Y., & Ueda, M. (2010). Cell Signaling Reactions: Single-molecule Kinetic Analyses. *Springer London*.

[9] Edman, L., & Rigler, R. (2000). Memory landscapes of single-enzyme molecules. *Proc Natl Acad Sci USA*, 97, 8266-8271.

[10] Kozuka, J., Yokota, H., Arai, Y., Ishii, Y., & Yanagida, T. (2006). Dynamic polymorphism of single actin molecules in the actin filament. *Nat Chem Biol*, 2, 83-86.

[11] Morimatsu, M., Takagi, H., Ota, K. G., Iwamoto, R., Yanagida, T., & Sako, Y. (2007). Multiple-state reactions between the epidermal growth factor receptor and Grb2 as observed using single-molecule analysis. *Proc Natl Acad Sci USA*, 104, 18013-18018.

[12] Sako, Y., & Yanagida, T. (2003). Single-molecule visualization in cell biology. *Nature Rev Mol Cell Biol*, 4, SS1-5.

[13] Sako, Y., Hiroshima, M., Park, G. C., Okamoto, K., Hibino, K., & Yamamoto, A. (2011). Live Cell Single-molecule Detection in Systems Biology. *WIREs Systems Biology and Medicine*, 4, 183-192.

[14] Hibino, K., Shibata, T., Yanagida, T., & Sako, Y. (2009). A RasGTP-induced conformational change in C-RAF is essential for accurate molecular recognition. *Biophys J*, 97, 1277-1287.

[15] Ueda, M., Sako, Y., Tanaka, T., Devreotes, P. N., & Yanagida, T. (2001). Single molecule anlaysis of chemotactic signaling in Dictyostelium cells. *Science*, 294, 864-867.

[16] Tani, T, Miyamoto, Y, Fujimori, E.K, Taguchi, T, Yanagida, T, Sako, Y, & Harada, Y. (2005). Trafficking of a ligand-receptor complex on the growth cones as an essential step for the uptake of nerve growth factor at the distal end of axon: a single-molecule analysis. *J Neurosci*, 25, 2181-2191.

[17] Uyemura, T., Takagi, H., Yanagida, T., & Sako, Y. (2005). Single-molecule analysis of epidermal growth factor signaling that leads to ultrasensitive calcium response. *Biophys J*, 88, 3720-3730.

[18] Tokunaga, M., Imamoto, N., & Sakata-Sogawa, K. (2008). Highly inclined thin illumination enables clear single-molecule imaging in cells. *Nat Meth*, 5, 159-161.

[19] Sako, Y. (2006). Imaging single molecules for systems biology. *Mol Syst Biol*, 10.1038/msb4100100.

[20] Betzig, E., Patterson, G. H., Sougrat, R., Lindwasser, O. W., Olenych, S., Bonifacino, J. S., Davidson, M. W., Lippincott-Schwartz, J., & Hess, H. F. (2006). Imaging intracellular fluorescent proteins at nanometer resolution. *Science*, 313, 1642-1645.

[21] Hibino, K., Hiroshima, M., Takahashi, M., & Sako, Y. (2009). Single-molecule imaging of fluorescent proteins expressed in living cells. *Methods MolBiol*, 48, 451-460.

[22] Yildiz, A., Forkey, J. N., McKinny, S. A., Ha, T., Goldman, Y. E., & Selvin, P. R. (2003). Myosin V walks hand-over-hand: single fluorophore imaging with 1.5-nm localization. *Science*, 300, 2061-2065.

[23] Murakoshi, H., Iino, R., Kobayashi, T., Fujiwara, T., Ohshima, C., Yoshimura, A., & Kusumi, A. (2004). Single-molecule imaging analysis of Ras activation in living cells. *Proc Natl Acad Sci USA*, 101, 7317-7322.

[24] Nguyen, V. T., Kamio, Y., & Higuchi, H. (2003). Single-molecule imaging of cooperative assembly of γ-hemolysis on erythrocyte membranes. *EMBO J*, 19, 4968-4979.

[25] Lemmon, M. A. (2009). Ligand-induced ErbB receptor dimerization. *Exp Cell Res*, 315, 638-648.

[26] Teramura, Y., Ichinose, J., Takagi, H., Nishida, K., Yanagida, T., & Sako, Y. (2006). Single-molecule analysis of epidermal growth factor binding on the surface of living cells. *EMBO J*, 25, 4215-4222.

[27] Hiroshima, M., Saeki, Y., Okada-Hatakeyama, M., & Sako, Y. (2012). Dynamically varying interactions between heregulin and ErbB proteins detected by single-molecule analysis in living cells. *Proc Natl Acad Sci USA*, 109, 13984-13989.

[28] Hibino, K., Watanabe, T., Kozuka, J., Iwane, A. H., Okada, T., Kataoka, T., Yanagida, T., & Sako, Y. (2003). Single- and multiple-molecule dynamics of the signaling from H-Ras to c-Raf1 visualized on the plasma membrane of living cells. *Chem Phys Chem*, 4, 748-753.

[29] Hibino, K., Shibata, T., Yanagida, T., & Sako, Y. (2011). Single-molecule kinetic analysis of RAF activation in the ternary complex among RAF, RasGTP, and the kinases on the plasma membrane of living cells. *J Biol Chem*, 286, 36460-36468.

[30] Nguyen, A. H., Nguyen, V. T., Kamio, Y., & Higuchi, H. (2006). Single-molecule visualization of environment-sensitive fluorophores inserted into cell membranes by Staphylococcal γ-hemolysin. *Biochemistry*, 45, 2570-2576.

[31] Groulx, N., Mc Guire, H., Laprade, R., Schwartz-L, J., & Blunck, R. (2011). Single molecule fluorescence study of the Bacillus thuringiensis toxin Cry1Aa reveals tetramerization. *J Biol Chem*, 286, 42274-42282.

[32] Nabika, H., Motegi, T., & Murakoshi, K. (2009). Single molecule tracking of cholera-toxin subunit B on GM1-ganglioside containing lipid bilayer. *e-J Surf Sci Nanotech*, 7, 74-77.

[33] Okumus, B., Arsian, S., Fengler, S. M., Myong, S., & Ha, T. (2009). Single molecule nanocontainers made porous using a bacterial toxin. *J Am ChemSoc*, 131, 14844-14849.

IntechOpen